Physica B 613 (2021) 412978

Contents lists available at ScienceDirect

Physica B: Physics of Condensed Matter

journal homepage: http://www.elsevier.com/locate/physb

Tuning photo-response and electronic behavior of graphene quantum dots synthesized via ion irradiation

Ashis K. Manna [a,b], Simeon J. Gilbert [c], Shalik R. Joshi [a,b], Takashi Komesu [c], Peter A. Dowben [c], Shikha Varma [a,b,*]

[a] Institute of Physics, Sachivalaya Marg, Bhubaneswar, Orissa, 751005, India
[b] Homi Bhabha National Institute, Training School Complex, Anushakti Nagar, Mumbai, 400085, India
[c] Department of Physics and Astronomy, Theodore Jorgensen Hall, 855 North 16th Street, University of Nebraska-Lincoln, Lincoln, NE, 68588-0299, USA

ARTICLE INFO

Keywords:
Graphene
Quantum dots
UV-Vis photo Response
Electronic behavior
Ion irradiation

ABSTRACT

The tuning of the photoresponse and electronic structure for ion induced graphene quantum dots (I-GQDs), through variations in the ion irradiation processing of monolayer graphene, is demonstrated. Synthesis of nano-dimensional quantum dots (3–9 nm) was observed for graphene after irradiation in the ion energy range of 100–250 eV. Remarkably, the photo-response from these GQDs can be manipulated and significantly enhanced simply with the change of ion energy. Changes to the photo-response are reflected in the appearance of an optical mode near 560 nm, and the enhancement of UV-regime absorbance by nearly 70%. The results display a method that can be useful in designing graphene quantum dot based photodetectors, in a single step process with ion irradiation, without incorporation of any metal-nanoparticles or hybrid-metal platforms. Changes in the UV absorbance are of immense significance having many potential applications in UV based detectors.

1. Introduction

Quantum structures have attracted considerable interest due to their nanometer size dependent optical and chemical properties. Graphene, while much studied and attractive for a number of potential applications [1], is not known for applications on the nanometer scale because of the problems caused by edge effects. Yet graphene on the nanometer scale opens up a band gap providing a route to a chemically inert material with interesting optical properties [1–4]. The result is that graphene quantum dots (GQDs) with nanoscale dimensions are receiving attention due to their promise related to photovoltaic devices, nanosecond life-time, bio-imaging, catalysis, molecular-scale electronic devices, light emitting devices and phototransistors [1–7]. However, there are severe limitations since GQDs do not express any visible-light absorption or prominent UV response unless they are doped, functionalized or integrated with metal nanoparticles [1,4].

Photonic devices based on graphene monolayer can exhibit great potential in optoelectronics due to its several exceptional characteristics like high optical transparency, strength and high carrier mobility [8]. Applications for photo devices in space communication, light modulators, photodetector, photovoltaic and photoemitters require good response in broadband wavelengths, ranging from visible to UV. As experimental realizations are challenging, several theoretical formalisms and simulations for improving performance and light trapping properties have been proposed [9–11]. Electromagnetic simulations of gold nanoparticle arrays incorporated in graphene show that surface plasmon resonance (SPR) activity, due to metal-nanoparticles, can tune the visible-range absorption phenomenon in graphene with nearly 30% improvement [9]. SPR has also been shown to enhance visible absorption by ten-fold in simulations that integrate light absorbing semiconductors in graphene [10]. A theoretical guide for the design of metal-dielectric-metal integrated structures with aluminum nanoparticles shows a 44% improvement in UV range [11]. Graphene/Ag nanocomposites prepared by reduction of graphene oxide (GO) display enhanced photo response in UV as well as visible range due to the formation of silver nanoparticles [12].

Efforts to synthesize GQDs have led to several ‘bottom up’ and ‘top down’ fabrication methods [1–6]. Both approaches suffer from some drawbacks: the former is usually more time consuming and requires many chemicals and reagents, whereas the latter involves multistep processes involving extremely high resolution lithography. Though several bottom-up routes like hydrothermal approach, organic synthesis

* Corresponding author. Institute of Physics, Sachivalaya Marg, Bhubaneswar, Orissa, 751005, India.
E-mail address: shikha@iopb.res.in (S. Varma).

https://doi.org/10.1016/j.physb.2021.412978
Received 12 November 2020; Received in revised form 8 January 2021; Accepted 9 March 2021
Available online 18 March 2021

and electrochemical technique have been used [3–6], fewer top down processes are available [2]. One of the initial top-down approaches applied the specialized technique of high resolution electron-beam lithography on 2D graphene to transform it into 0D quantum dots [2]. Peng et al. have utilized wet chemical method to derive GQDs from the acidic treatment of Carbon fibers [7]. The breakup of the fiber structure and chemical fracture of the planar graphitic domains induces the formation of GQDs whose size and UV absorption response varies with reaction temperatures [7]. Layered structures of nitrogen doped graphene Quantum dots [6], prepared using glucose and ammonia as sources in a microwave assisted method, demonstrate a size dependent broad-band photo response. In another solution chemistry derived approach, phenyl moieties are appropriately attached to the graphene edges for controlling the shape and size of GQDs for enhancing the absorption edge [5]. Li et al. have shown that the GQDs prepared via an electrochemical route [4] are stable and display a UV adsorption band in water medium.

Ion irradiation, with the potential for the controlled introduction of energetic ions [38,39], provides an alternative simple top-down route for modifications of graphene [13–18]. Lucchese et al. applied 90 eV Ar^+ ion irradiation, with varying fluences, to investigate the synthesis of nano-crystallites in monolayer graphene [17]. However, technological manifestations of irradiated graphene for photosensitive applications have never been investigated.

In the present paper, we discuss the photo-response and changing chemical configuration for ion induced graphene quantum dots (I-GQDs). These GQDs, prepared by ion irradiation of monolayer graphene, show nano-dimensional sizes (3–9 nm) that can be interestingly manipulated with variation in ion energy. The accompanying UV–Vis photo-response demonstrates many fascinating behaviors including appearance of a new broad optical mode near 560 nm due to the presence of I-GQDs. Another remarkable feature is nearly 70% enhancement in UV-response. Other characteristic UV-absorption modes attributed to the π (or n) to π* plasmonic transitions also appear after irradiation. Simulation and theoretical model suggest [9–12] improved light absorption characteristics for graphene when integrated with metal and semiconductor nanoparticles. On the experimental front, functionalization and doping are some of the important routes discussed for enhancing light trapping in GQDs [3–7]. Yet, synthesis via chemical and solution based methods often require multiple processing steps. In the present study, a single step process of ion irradiation has been applied to fabricate I-GQDs that play crucial role in engineering photo-absorption properties which have been achieved here in the absence of doping, functionalization or incorporation of any metal nanoparticles in graphene. To our knowledge, the photo-response in graphene or GQDs synthesized via ion irradiation of graphene, has not been previously explored.

2. Experimental section

2.1. Sample preparation

Single layer graphene samples were commercially procured from Graphenea (Spain). The monolayer graphene was used as-received on SiO_2/Si substrates. Implantation of graphene films was carried out at RT with Ar^+ ions at normal incidence. Chamber pressure was maintained at 5×10^{-6} Torr. In order to assess the role of ion energy, the ion implantation was performed at various ion energies of 100, 150, 200, 250 and 300 eV. The fluence of ions was kept constant at 2.2×10^{14} ions/cm^2. The flux was 3.7×10^{12} ions/cm^2.sec. The ion beam was scanned over the sample, in order to achieve uniform implantation. The lowest ion energy of 100 eV is just sufficient to overcome the C atom displacement threshold, without causing any cascading effect [19,20].

2.2. Characterization

XPS was performed in an ultra-high vacuum (UHV) chamber which is equipped with an Al K_α source (1486.6 eV) and a VG100AX hemispherical analyzer. The base pressure of the system was better than 1×10^{-9} Torr at room temperature. All XPS spectra were collected at normal photoelectron emission to the sample surface. The optical properties of graphene and ion irradiated graphene surfaces were investigated by a UV–Vis spectrophotometer (CARY 5000) equipped with integrating sphere and using BaSO4 as a standard. Diffuse reflectance absorption (DRA) studies were carried out on the graphene/SiO_2/Si samples.

The Raman scattering studies were performed in backscattering geometry on a T64000 triple monochromator Horiba Jobin Yvon system equipped with a liquid nitrogen cooled CCD detector. Raman spectra were carefully acquired with a 514 nm (2.41 eV) laser. The power of the laser was below 1 mW and the resolution of the system was 0.5 cm^{-1}. Analysis of modes is presented here, after fitting with Lorentzian profiles.

The morphology of the ion irradiated surfaces was also investigated by Atomic Force Microscopy (AFM) using a Nanoscope V (Bruker) in the tapping mode.

3. Results and discussion

3.1. Defect creation

Fig. 1 shows the Raman Spectra acquired for pristine as well as ion irradiated graphene, the latter at several ion energies. Characteristic Raman fundamental G and 2D modes of graphene are expected in the range of 1580–1600 and near 2600 cm^{-1}, respectively [16,21,22]. The pristine graphene shows presence of these modes, in Fig. 1, at 1583.5 cm^{-1} and 2680.5 cm^{-1}, respectively. A very tiny D mode near 1345 cm^{-1} can be attributed to the graphene edges [18]. The second order 2D Raman band displays a very high intensity and I_{2D}/I_G of ~2.8, confirming the existence of a good quality graphene monolayer.

Irradiation introduces vacancy type defects in the graphene lattice [23]. This is very evident in the Raman spectra. Visible Raman

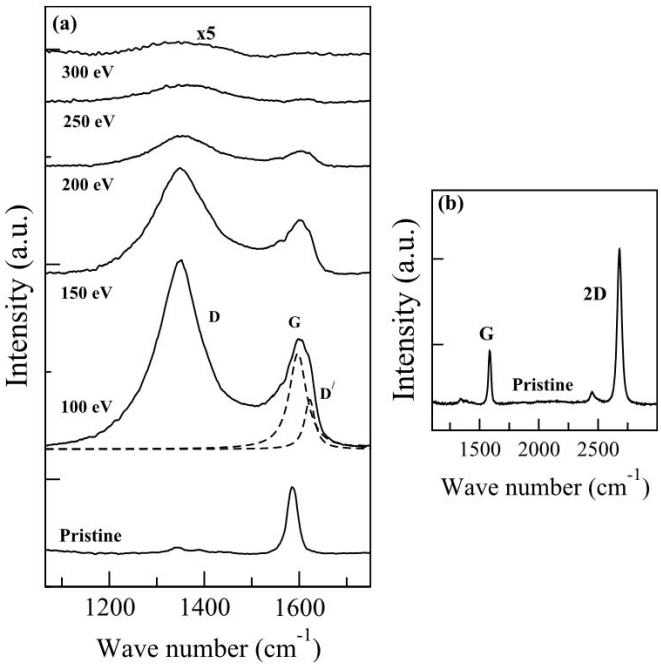

Fig. 1. (A) Raman spectra after irradiation of graphene at various ion energies. The ion irradiation fluence was kept constant at 2.2 x 10^{14} ions/cm^2. (b) Raman spectrum from pristine graphene showing G and 2D modes.

spectroscopy is efficient in probing the graphene sp^2 bonds since their π states get highly excited by the visible photons [4,22]. Such influence of the graphene π bond on the Raman spectra is largest when the π bonds occur in aligned pair configurations like six membered rings or clusters of such six membered rings. This is altered after ion irradiation. After irradiation of graphene with 100 eV Ar^+ ions, the Raman spectra in the region of G mode broadens so that both D and D' modes are observed, as is evident in Fig. 1. The D'mode appears as a shoulder to the G mode and these two modes were de-convoluted (see Fig. 1). Similar behavior has also been observed earlier after the irradiation of graphene with swift heavy ions [24]. The evolution of the height of the G mode, after deconvolution, is displayed in Fig. 2. With ion irradiation at modest ion energies (100 eV), the intensity of the G mode Raman feature does not change much from pristine graphene. After irradiation at higher ion energy beyond 100 eV, there is a systematic decrease of the G mode Raman feature. The in-plane stretching of C-sp^2 atoms, in chains as well as rings, contribute to the G mode in Raman. Since this corresponds to the relative stretching vibrations of sp^2 atoms, it does not require the presence of the six membered or any other rings. This explains the presence of a significant G peak after irradiation at an ion energy beyond 100 eV, while the decrease in the G peak at higher ion energies indicates modifications in the lattice due to the distortion of sp^2 sites [13,16].

Fig. 2 displays the height of the D mode as it evolves under ion irradiation. This mode results from the breathing mode of six membered carbon rings and becomes more active in the presence of defects [13,22]. This is consistent with the significant increases in this Raman feature with ion irradiation at modest ion energies (100 eV and 150 eV), as plotted in Fig. 2. Though the contributions of long ranged polarization effects in π states from six membered rings add constructively towards the intensity, those from the other order rings cancel this effect and induce lowering of the Raman D mode intensity. At lower energies, the increase in the Raman D mode intensity is due to the incorporation of point defects [17]. The D band becomes activated via the breathing modes of six-membered rings and the decrease in the D band intensity, for ion irradiation energies beyond 100 eV, reflects the distortion of these rings along with the creation of lower order rings and their clusters [13,17]. Thus with sufficient damage to the graphene, through ion irradtion, the D mode intensity seen at lower ion irradiation energies cannot be sustained. After irradiation at ion energy of 300 eV, all the modes diminish substantially, but in the same proportion. These investigations have been carried out at a constant ion irradiation fluence of 2.2 × 10^{14} ions/cm^2 and only the variations in ion energy are responsible for modifications shown here. This is in contrast to most other studies where usually the role of ion fluence is investigated. These results indicate a substantial influence of ion energy in the lattice modulation.

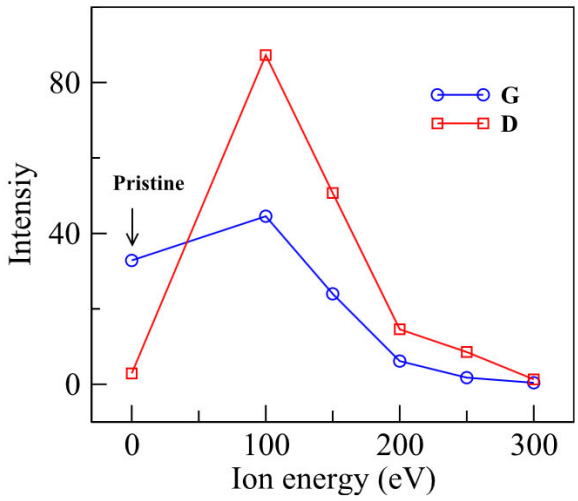

Fig. 2. Evolution of heights for Raman G and D modes after implantation at various ion energies. The ion irradiation fluence was kept constant at 2.2 x 10^{14} ions/cm^2.

Fig. 3 shows the ratio I_D/I_G as a function of ion energy, with I_D and I_G being the intensities of the D and G modes, respectively. The ratio is very small, as expected, for the pristine but rises significantly with increasing ion energy up to 250 eV. Rise in I_D/I_G corresponds to ion induced disorder resulting from the influence of the opening of graphene sp^2 ring configurations yielding sp^3 conformations and distorted sp^2 clusters [4, 17]. As a consequence, the size of ordered sp^2 hybridized graphene crystallites (L_a) decrease [25,26]. This, as discussed below, promotes the synthesis of nano-dimensional quantum confined GQDs. The final inflexion in the ratio at 300 eV reflects (Fig. 3) the initiation of amorphization in graphene [13,23,25]. This increased amorphous graphitic content contributes to the increased in sp^3 content, as is also evident in the destruction of the D mode breathing vibrations. XPS investigations presented below also confirm these observations.

3.2. Graphene cluster size

The in-plane correlation length or the diameter (L_a) of the sp^2 graphene clusters can be estimated using the Tuinstra and Koening (T-K) relation which is inversely related to the Raman D and G mode intensity ratio I_D/I_G [27]. The T-K relation is given as [13,27]:

$$L_a = \left[2.4 \times 10^{-10} \lambda^4 \left(\frac{I_D}{I_G}\right)^{-1} nm^{-3}\right] \quad (1)$$

Here λ is the wavelength of the excitation laser in nm.

Fig. 4 displays the estimated graphene crystallite size and correlation length L_a which is reduced to nearly 7–9 nm after irradiation with 100–200 eV ions. For 90 eV ion irradiation of monolayer graphene, investigated for varying fluences, similar L_a has been reported [17]. Here, the ion irradiation induced graphene quantum dots (I-GQDs) exhibit a further reduction in size (L_a ~3.5 nm) after irradiation with an ion energy of 250 eV (Fig. 4). After 300 eV irradiation, initiation of amorphization occurs (as seen in Fig. 3) and the T-K relation is no longer applicable [13,16]. These results are consistent with the atomic force microscopy studies presented below.

Surface morphologies from the pristine and ion irradiated graphene, obtained from high resolution AFM images, are shown in Fig. 5. After 100 eV irradiation, several bright regions appear in the AFM images which can be attributed to the disordering. Similar morphologies have been observed for graphene irradiated with Ar^+ ions of 90 eV [17]. The disordered regions reflect the destruction in the ordered sp^2 rings into distorted sp^2 and sp^3 sites [28]. Using these AFM images, the size of undamaged graphene can be measured which provides an estimate of L_a,

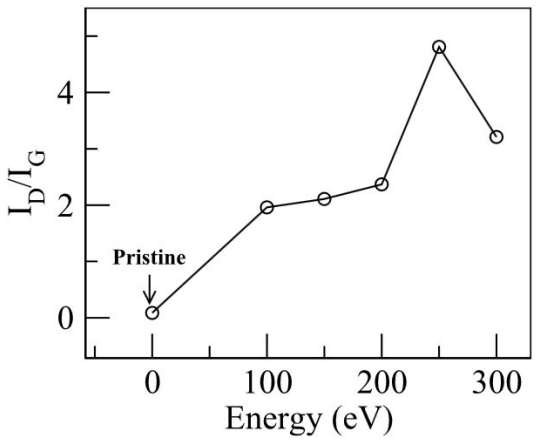

Fig. 3. Ratio of Raman D and G mode intensities, I_D/I_G, as a function of ion energy. The ion irradiation fluence was kept constant at 2.2 x 10^{14} ions/cm^2.

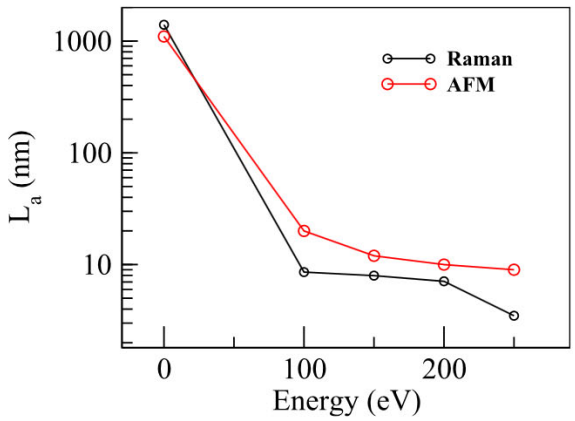

Fig. 4. Size L_a measured from Raman (using T-K relation) and AFM are shown, as a function of ion energy. The ion irradiation fluence was kept constant at 2.2 x 10^{14} ions/cm^2.

as shown in Fig. 4. For 200 eV and higher energies, some coalescence of the disordered regions is also observed (Fig. 5) causing a mild decrease in L_a. The correspondence between L_a measured by Raman and AFM techniques is shown in Fig. 4. One notices that AFM overestimates the size slightly, as expected due to the fact that regions close to the defect will also be slightly disordered and should not be included in the calculation.

Evolution of ion irradiated graphene, investigated here with varying ion energy, displays two significant transformations. First, after 100 eV irradiation, a transition from graphene to nano-dimensional I-GQDs occurs. With increasing ion energy, these dots decrease in size and surprisingly at 300 eV some amorphization is introduced. Amorphization has been noticed in ion irradiated graphene, for fluence dependent investigations, with 30 keV N^+ [23] and 30 keV Ga ions [13].

3.3. *The changing electronic structure of graphene with ion irradiation*

XPS is a powerful technique for understanding the chemical species on the surface. It has been utilized to assess the sp^2 and sp^3 bonded carbon content as well as the presence of oxygen functional groups on the graphene surface. The spectra shown here are clearly dependent on the energy of irradiation. The C (1s) spectrum, from the pristine graphene (Fig. 6) can be fitted with four features related to C═C (284.8 eV), C–OH (285.7 eV), C–O (286.6 eV) and C═O (287.5 eV) [2,6,25,29]. The primary C═C feature corresponds to the sp^2 component in graphene and its high intensity indicates a good graphene monolayer. All the three types of oxygen functional groups, namely single bonded hydroxyl group (C–OH), epoxide group (C–O) as well as the double bonded carbonyl group (C═O) are observed on the pristine graphene. These components within the C 1s envelope could be partly the result of impurity carbon species. While impurity carbon species cannot be excluded, of key interest here is the ratio sp^3/sp^2, as a function of ion energy.

After 100 eV irradiation, the XPS profile displays a new feature at 285.5 eV, not present in pristine graphene. This corresponds to the formation of sp^3 conformations due to the opening up of ordered sp^2 ring configurations [30,31]. Interestingly, the ratio sp^3/sp^2 illustrates (Fig. 6e) similar behavior as I_D/I_G (in Fig. 3), except at 300 eV where declining I_D/I_G in Raman indicates a cross-over to the initial stages of amorphization. The difference can be accounted by the fact that visible Raman spectroscopy is preferentially sensitive to sp^2, rather than sp^3, states. Rise in sp^3 content (Fig. 6), with ion energy, introduces the confinement of sp^2 ring clusters, contributing to the synthesis of I-GQDs in graphene after ion irradiation.

The UV–Vis spectrum of pristine graphene (Fig. 7) displays the prominent exciton –shifted van Hove singularity in the graphene density of state [26]. The corresponding mode at 250 nm reflects the $\pi-\pi^*$ transition of sp^2 bonded carbon, and sometimes result in a satellite feature in XPS [31]. The characteristic monolayer graphene is also corroborated by the near wavelength-independent absorption on approaching 800 nm [4,8,9,26].

After ion irradiation, the absorption spectra exhibit a number of modifications, most significant being a much higher overall photo response, compared to pristine. Surprisingly after 150 eV ion irradiation, UV absorbance illustrates a nearly 70% enhancement. Additionally, three new near UV absorption features, located near 210, 250 and 330 nm can be seen. These modes correspond to π (or n) to π^* plasmonic transitions [4,12,32,33] and have been observed for nitrogen doped GQDs that were synthesized in a multi-step solution process [6] as well as in DFT studies for boron doped GQDs [34]. The main van Hove singularity related feature, near 250 nm, continues to be intense (Fig. 7) but displays a small redshift with increasing ion energy. After 250 eV ion irradiation, the UV-response reduces significantly, compared to pristine, though it is still very high in the other wavelength range (350–800 nm). A much diminished and nearly featureless photo-response is observed after the 300 eV ion energy irradiation. This is expected [35] given that we understand from Raman and XPS results that a significant increase in the amorphous and sp^3 content occurs at this stage. Presence of mild interference fringes also indicate the change in the refractive index of graphene monolayer due to the increased amorphization [36]. Results presented here reveal that ion energy plays crucial role in modulating the absorption properties of graphene upon irradiation. Significantly, these have been achieved via the synergetic irradiation of graphene which introduces confinement of sp^2-C domains leading to the synthesis of I-GQDs.

Another important aspect in the photo-response is the appearance of a visible mode near 560 nm. Appearance of this mode reflects the

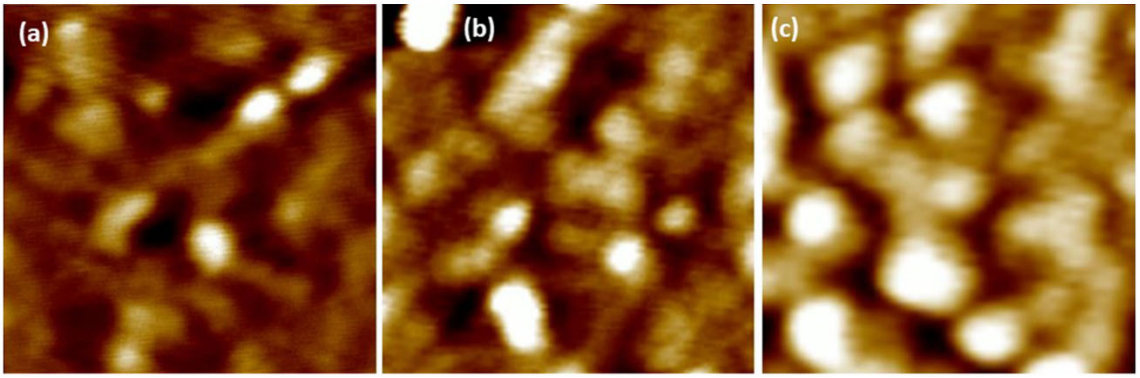

Fig. 5. High resolution 200 × 200 nm^2 AFM image from graphene after irradiation with (a) 100 eV, (c) 200 eV and (c) 300 eV. The ion irradiation fluence was kept constant at 2.2 x 10^{14} ions/cm^2.

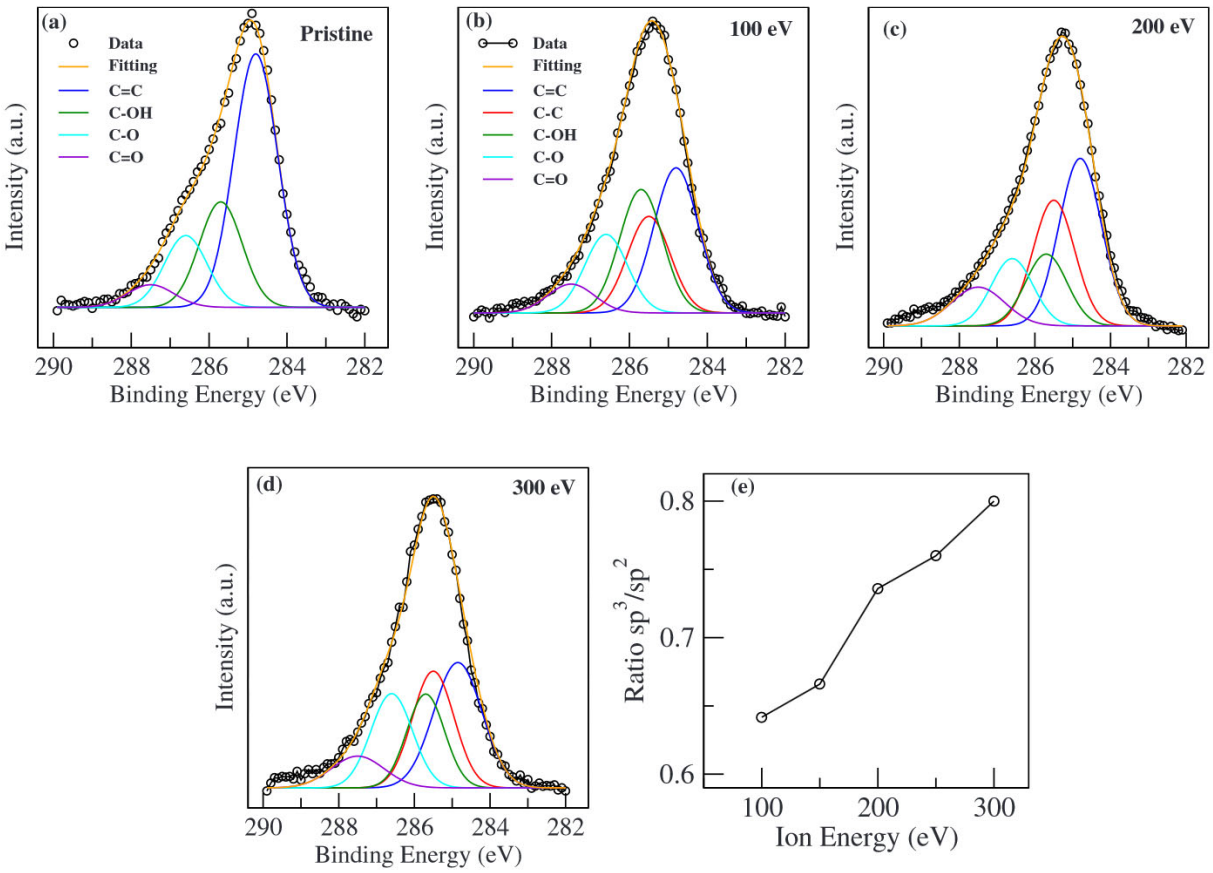

Fig. 6. C (1s) core level XPS spectra from graphene (a) pristine and after irradiation with (b) 100 eV (c) 200 eV and (d) 300 eV. (e) Ratio sp^3/sp^2 for graphene irradiated at various ion energies. The ion irradiation fluence was kept constant at 2.2 x 10^{14} ions/cm^2.

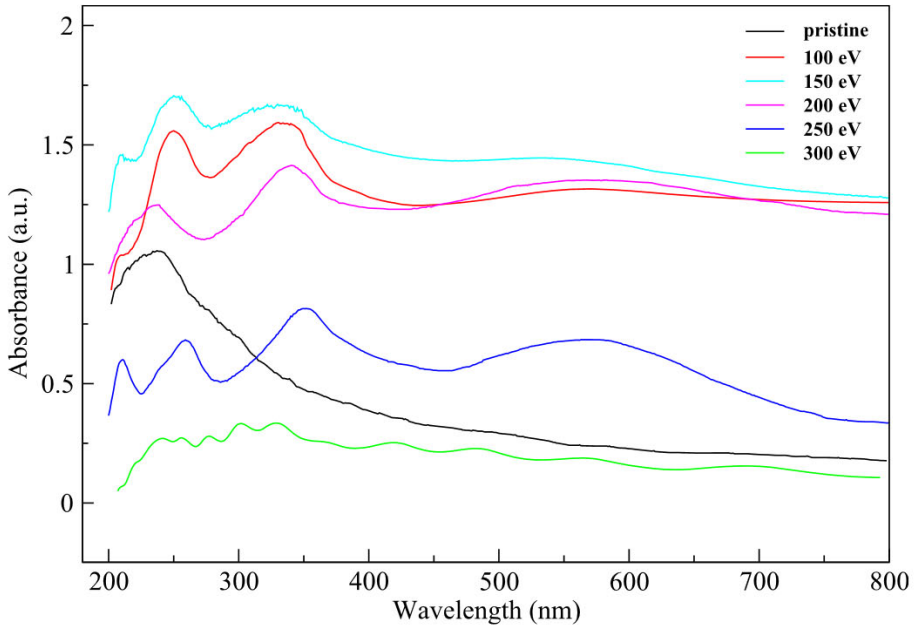

Fig. 7. The UV–Vis optical absorption spectra for graphene irradiated at various ion energies. The ion irradiation fluence was kept constant at 2.2 x 10^{14} ions/cm^2.

opening of the bandgap in graphene upon ion irradiation of graphene. Exhibiting a broad absorption band from 450 nm to 700 nm, this mode is weak at lower irradiation energies (100–200 eV). Still, its intensity is much higher (125%) compared to the pristine. This mode becomes very prominent after 250 eV irradiation. With the inclusion of silver nanoparticles in graphene, surface plasmon resonance (SPR) phenomenon in Ag-graphene nanocomposite shows a band near 400 nm [12]. Simulations for gold nanoparticle arrays incorporated in graphene estimate 30% enhancement in absorption near 620 nm [9]. In the present case, however, there are no metal nanoparticles and the origin of this

optical mode is related to the synergetic synthesis of I-GQDs via ion irradiation in graphene. Presence of such optical bands in graphene, upon ion irradiation, have never been explored.

The highest visible-intensity (125%) has been observed after irradiation at lower ion energies. This is expected due to the presence of larger sized I-GQDs, with L_a ranging from 7 to 9 nm (Fig. 4). As the size of dots decreases after 250 eV irradiation, the response reduces but the absorption peak becomes very prominent. Nitrogen doped GQDs prepared in solution using ammonia show a broad optical band [6]. GQDs prepared by several other methods, as well as carbon nanoparticles, do not show any visible absorption unless they are doped, functionalized or integrated with metal nanoparticles [1,4,37]. Thus, the quantum confined nanostructure, achieved here via the synergetic irradiation of graphene, presents very rich and interesting absorption characteristics with the variation of ion energy.

4. Conclusions

The present study discusses the photo response and the electronic behavior of the ion irradiated monolayer graphene that contributes to the synthesis of GQDs. The results demonstrate that ion energy is a crucial parameter that can effectively modulates the size of the GQDs as well as many other characteristic properties. Along with tuning the size of I-GQDs at lower (100–250 eV) ion energies, initiation of amorphization at 300 eV is observed. After irradiation, the UV–Vis absorbance displays multiple surprising behaviors. Most significantly, a broad optical mode near 560 nm is observed that can be attributed to the presence of I-GQDs. Remarkably, a large 70% enhancement in UV-absorption as well as two new UV modes attributed to the π (or n) to π* plasmonic transitions also appear. Although many chemical and solution based techniques have been applied to the preparation of GQDs, those usually demand multiple steps and the properties displayed by such dots are influenced by a variety of process parameters. The advantage of the present approach demonstrates that the single step ion irradiation of monolayer graphene results in I-GQDs whose response can be manipulated by ion energy. These I-GQDs present many exceptional light absorption properties which have been achieved here in the absence of any dopant, plasmonic metal nanoparticles or metal semiconductor hybrid layers. Ion irradiation has thus been used to manipulate the electronic and absorption behavior in graphene which can act as a platform for applications in photo detection. These results could have a significant impact in designing conjugated Visible and UV range photodetectors from graphene quantum dots and tuning the GQD photoresponse.

Author contribution

Ashis K. Manna: Formal analysis, Investigation, Writing – review & editing, Simeon J. Gilbert: Formal analysis, Investigation, Writing – review & editing, Shalik R. Joshi: Investigation, Writing – review & editing, Takashi Komesu: Investigation, Writing – review & editing, Peter A. Dowben: Supervision, Conceptualization, Writing – review & editing, Shikha Varma: Supervision, Conceptualization, Writing – review & editing,

Declaration of competing interest

The authors declare that they have no known competing financial interests or personal relationships that could have appeared to influence the work reported in this paper.

Acknowledgements

S.V. and A.M. would like to acknowledge the financial help received from the Department of Science and Technology - Science and Engineering Research Board (DST-SERB), India (No. DST/EMR/2016/000728). This work was also partly funded by the Nebraska Public Power District through the Nebraska Center for Energy Sciences Research at the University of Nebraska-Lincoln, NCESR grant number 19-SE-2018. Authors thank Prof. T. Som for Ion Irradiation facility. Help of Mr. Santosh Choudhury with Raman spectroscopy is acknowledged.

References

[1] J.B. Wu, M.L. Lin, X. Cong, H.N. Liu, P.H. Tan, Chem. Soc. Rev. 47 (2018) 1822–1873.
[2] L.A. Ponomarenko, F. Schedin, M.I. Katsnelson, R. Yang, E. Hill, K.S. Novoselov, A. K. Geim, Science 320 (2008) 356–358.
[3] Y. Li, Y. Hu, Y. Zhao, G. Shi, L. Deng, Y. Hou, L. Qu, Adv. Mater. 23 (2011) 776–780.
[4] V. Georgakilas, J.A. Perman, J. Tucek, R. Zboril, Chem. Rev. 115 (2015) 4744–4822.
[5] X. Yan, X. Cui, B. Li, L. Li, Nano Lett. 10 (2010) 1869–1873.
[6] L. Tang, R. Ji, X. Li, G. Bai, C.P. Liu, J. Hao, J. Lin, H. Jiang, K.S. Teng, Z. Yang, S. P. Lau, ACS Nano 8 (2014) 6312.
[7] J. Peng, W. Gao, B.K. Gupta, Z. Liu, R.R. Aburto, L. Ge, L. Song, L.B. Alemany, X. Zhan, G. Gao, S.A. Vithayathil, B.A. Kaipparettu, A.A. Marti, T. Hayashi, J. J. Zhu, P.M. Ajayan, Nano Lett. 12 (2012) 844–849.
[8] R.R. Nair, P. Blake, A.N. Grigorenko, K.S. Novoselov, T.J. Booth, T. Stauber, N.M. R. Peres, A.K. Geim, Science 320 (2018) 1308.
[9] J. Zhu, Q.H. Liu, T. Lin, Nanoscale 5 (2013) 7785.
[10] S. Xiao, T. Wang, X. Jiang, B. Wang, C. Xu, Plasmonics 13 (2018) 897.
[11] Y. Cai, Z. Wang, S. Yan, L. Ye, J. Zhu, Opt. Mater. Express 8 (2018) 3295.
[12] Z. Ciplak, N. Yildiz, A. Calimli, Fullerenes, Nanotub. Carbon Nanostruct. 23 (2014) 361–370.
[13] Y.B. Zhou, Z.M. Liao, Y.F. Wang, G.S. Duesberg, J. Xu, Q. Fu, X.S. Wu, D.P. Yu, J. Chem. Phys. 133 (2010) 234703.
[14] L. Tapasztó, G. Dobrik, P.N. Incze, G. Vertesy, P. Lambin, L.P. Biró, Phys. Rev. B 78 (2008) 233407.
[15] A.H.N. Castron, F. Guinea, N.M. Perer, A.K. Geim, Rev. Mod. Phys. 81 (2009) 109.
[16] A.C. Ferrari, J. Robertson, Phys. Rev. B 61 (2000) 14095–14107.
[17] M.M. Lucchese, F. Stavale, E.H.M. Ferreira, C. Vilani, M.V.O. Moutinho, R. B. Capaz, C.A. Achete, A. Jorio, Carbon 48 (2010) 1592–1597.
[18] R. Beams, L.G. Canc-ado, L. Novotny, Nano Lett. 11 (2011) 1177–1181.
[19] J.R. Hahn, H. Kang, Phys. Rev. B 60 (1999) 6007–6017.
[20] D. Marton, H. Bu, K.J. Boyd, S.S. Todorov, A.H. Al-Bayati, J.W. Rabalais, Surf. Sci. Lett. 326 (1995) 489–493.
[21] A. C Ferrari, J.C. Meyer, V. Scardaci, C. Casiraghi, M. Lazzeri, F. Mauri, S. Piscanec, D. Jiang, K.S. Novoselov, S. Roth, A.K. Geim, Phys. Rev. Lett. 97 (2006) 187401.
[22] L.M. Malard, M.A. Pimenta, G. Dresselhaus, M.S. Dresselhaus, Phys. Rep. 473 (2009) 51–87.
[23] B. Guo, Q. Liu, E. Chen, H. Zhu, L. Fang, J.R. Gong, Nano Lett. 10 (2010) 4975–4980.
[24] N.A. Nebogatikova, I.V. Antonova, S.V. Erohin, D.G. Kvashnin, A. Olejniczak, V. A. Volodin, A.V. Skuratov, A.V. Krasheninnikov, P.B. Sorokin, L. A. Chernozatonskii, Nanoscale 30 (2018) 14499–14509.
[25] E. Casero, C. Alonso, L. Vazquez, M.D. Petit-Dominguez, A.M. Parra-Alfambra, M. de la Fuente, P. Merino, S. Alvarez-Garcia, A. de Andres, F. Pariente, E. Lorenzo, Electroanalysis 25 (2013) 154–165.
[26] F. Bonaccorso, Z. Sun, T. Hasan, A.C. Ferrari, Nat. Photonics 4 (2010) 611–622.
[27] F. Tuinstra, J.L. Koening, J. Chem. Phys. 53 (1970) 1126.
[28] M.A. Abdol, S. Sadeghzadeh, M. Jalaly, M.M. Khatibi, Sci. Rep. 9 (2019) 8127.
[29] L. Kong, C. Bjelkevig, S. Gaddam, M. Zhou, Y.H. Lee, G.H. Han, H.K. Jeong, N. Wu, Z. Zhang, J. Xiao, P.A. Dowben, J.A. Kelber, J. Phys. Chem. C 114 (2010) 21618–21624.
[30] L. Stobinski, B. Lesiak, A. Malolepszy, M. Mazurkiewicz, B. Mierzwa, J. Zemek, P. Jiricek, I. Bieloshapk, J. Electron. Spectrosc. Relat. Phenom. 195 (2014) 145–154.
[31] S.W. Kim, H.K. Kim, K. Lee, K.C. Roh, J.T. Han, K.B. Kim, S. Lee, M.H. Jung, Carbon 142 (2019) 373–378.
[32] M. Zhou, F.L. Pasquale, P.A. Dowben, A. Boosalis, M. Schubert, V. Darakchieva, R. Yakimova, L. Kong, J.A. Kelber, J. Phys. Condens. Matter 24 (2012), 072201.
[33] Q. Lai, S. Zhu, X. Luo, M. Zou, S. Huang, AIP Adv. 2 (2012), 032146.
[34] J. Feng, H. Dong, B. Pang, Y. Chen, L. Yu, L. Dong, Mater. Chem. C 7 (2019) 237–246.
[35] Q. Liang, C. Yan, Y. Meng, J. Lai, S. Krasnicki, H. Mao, R.J. Hemley, J. Phys. Condens. Matter 21 (2009) 364215.
[36] L. Gao, F. Lemarchand, M. Lequime, J. Europ. Opt. Soc. Rap. Public. 8 (2013) 13010.
[37] L. Cao, S. Sahu, P. Anilkumar, C.E. Bunker, J. Xu, K.A.S. Fernando, P. Wang, E. A. Guliants, K.N. Tackett, Y. Sun, J. Am. Chem. Soc. 133 (2011) 4754–4757.
[38] Soma Dey, C Roy, A Pradhan, Shikha Varma, J. Appl. Phys. 87 (2000) 1110.
[39] Subrata Majumder, D Paramanik, V Solanki, B Bag P, Shikha Varma, Appl. Phys. Lett. 98 (2011) 053105.